University of Groningen

Ferroelectricity-functionalized organic field-effect transistors

Naber, Ronald Cornelis Gerard

IMPORTANT NOTE: You are advised to consult the publisher's version (publisher's PDF) if you wish to cite from it. Please check the document version below.

Document Version
Publisher's PDF, also known as Version of record

Publication date:
2006

Link to publication in University of Groningen/UMCG research database

Citation for published version (APA):
Naber, R. C. G. (2006). *Ferroelectricity-functionalized organic field-effect transistors*. s.n.

Copyright
Other than for strictly personal use, it is not permitted to download or to forward/distribute the text or part of it without the consent of the author(s) and/or copyright holder(s), unless the work is under an open content license (like Creative Commons).

The publication may also be distributed here under the terms of Article 25fa of the Dutch Copyright Act, indicated by the "Taverne" license. More information can be found on the University of Groningen website: https://www.rug.nl/library/open-access/self-archiving-pure/taverne-amendment.

Take-down policy
If you believe that this document breaches copyright please contact us providing details, and we will remove access to the work immediately and investigate your claim.

Downloaded from the University of Groningen/UMCG research database (Pure): http://www.rug.nl/research/portal. For technical reasons the number of authors shown on this cover page is limited to 10 maximum.

Download date: 04-05-2023

Voorwoord

Dit proefschrift gaat over de mogelijkheid om een ferroelektrisch polymeer te gebruiken om organische veld effect transistoren te maken met bijzondere extra functionaliteiten. De hoofdstukken zijn origineel geschreven als publicaties in internationale bladen. De volgorde van de hoofdstukken is gelijk aan de chronologische volgorde waarin de bevindingen gedaan zijn. Dit is een handige volgorde omdat bijvoorbeeld de experimenten die beschreven staan in hoofdstuk 7 pas goed gedaan konden worden na de ervaringen die (deels) beschreven staan in hoofdstukken 4 tot en met 6. De chronologische volgorde geeft de lezer wellicht ook een idee van het leerproces dat zich heeft plaatsgevonden tijdens het promotieonderzoek.

Tijdens een promotieonderzoek is goede aansturing en samenwerking onontbeerlijk. Hiervoor wil ik graag een aantal mensen bedanken. Paul, bedankt voor de goede begeleiding en werksfeer, het bedenken en medebedenken van vele onderzoeksideeën en de goede technische faciliteiten in de groep. Dago zou ik graag willen bedanken voor de goede samenwerking, de wetenschappelijke bijdrages en de interesse voor alle aspecten van het onderzoek. Voor veel experimenten was de technische kennis van Minte, met hulp van Joop en later Jan, onontbeerlijk. Bert heeft drie hoofdstukken van dit proefschrift mogelijk gemaakt met zijn gezuiverde P3HT en hij was een interessante discussiepartner om ideeën mee uit te wisselen. Jurjen was altijd bereid te helpen met chemische vragen. Voor al deze dingen dus mijn dank.

De goede sfeer in het lab en daarbuiten was er mede dankzij alle (ex-)labratten (en hun partners) binnen en buiten de groep: Teunis, Cristina, Valy, Denis, Magda, Jan Anton, Afshin, Hylke, Edsger, Kamal, Francesco, Martijn, Andre, Herman, Jan, Coen, Marten, Hans, Gerke, Sander, Anneloes, Leendert, Henk, Marie, Jos, Onno en Maaike. Cristina, Afshin, Hylke en Kamal wil ik daarnaast bedanken voor de goede samenwerking. Hessel, Joost, Martijn, Johan en Mark Jan wil ik bedanken voor hun inzet tijdens hun afstudeerprojecten. Van de ondersteunende diensten wil ik graag Renate, Linda en Nanno bedanken voor hun rol. Als laatste wil ik mijn moeder, Ibella, mijn vader, mijn zus en Sybren bedanken voor alles.

Introduction

i. Motivation

This thesis addresses the possibility of using organic materials to make a nonvolatile memory device by combining a ferroelectric and a semiconductive polymer. It is conceivable that such a memory device could be made by solution-processing techniques, which would enable its use in ultra-low-cost applications. One of the main applications that one can conceive for such polymer memory devices is low-cost mass data storage. For this application it would have to compete with Flash memory technology (currently a multibillion euro market) by offering lower production costs. Another major application is integrated memory. An important example of this is the plastic RFID (radio-frequency identification) tag. These tags are small integrated circuits that communicate with a reader via radio communication, to send and receive information stored in its memory. The intended purpose of the plastic tags is to replace bar codes. RFID tags produced by traditional silicon technologies cost at least €0.25 per tag. In order to compete with bar codes, it is estimated that the purchase price of the tags must come down to a few cents or less. This is unattainable with traditional silicon technology, but it may be possible to achieve this by using organic materials that are processed with low-cost solution-based techniques. These low-cost RFID tags could have spin-off applications in many areas: The package transport sector could use them to track items; Food packages could be tagged so that a computerized refridgerator could sense its own contents and give a warning when a product has reached its use-by date; Medicine packages could be tagged to enable an automated way of checking whether patients are taking their medication. In order to explain how the device is supposed to work, we first introduce ferroelectricity and ferroelectric polymers. This is followed by conjugated polymer semiconductors and their charge transport properties in field-effect transistors. We end with an introduction to the polymer ferroelectric field-effect transistor, which was the main aim of the work, and a short summary of the thesis.

ii. Ferroelectric thin film capacitors

Ferroelectricity was discovered in 1922 in Rochelle salt ($KNa(C_4H_4O_6)\cdot 4H_2O$). It was found that the "electrical properties of Rochelle salt crystal are analogous to the magnetic properties of iron, the dielectric displacement D and polarization P varying with the electric field E in the same general manner as B and I vary with H for iron, and showing an electric hysteresis with loops distorted by an amount corresponding to the permanent polarization

P_0" [1]. Ferroelectricity remained a curiosity for a long time after 1922 because there were only two known ferroelectric materials: Rochelle salt and potassium dihydrogen phosphate (KH_2PO_4) [2]. The discovery of ferroelectricity in barium titanate ($BaTiO_3$) in 1944 and other ceramics in later years, most notably the lead zirconate titanate ($Pb(Zr,Ti)O_3$, PZT) family of materials, induced a surge in research efforts toward the phenomenon. These modern ferroelectric materials are now used for a vast array of applications including transducer, acoustic sensor and memory. Ferroelectrics are also used as model systems for studying solid-solid phase transitions by taking advantage of the ferroelectric-paraelectric phase transition at the Curie temperature.

Let us consider two metal plates in close proximity in a vacuum. With a voltage difference V applied to the plates, an electric field E arises in the vacuum equal to

$$E = \frac{-V}{d}, \qquad (1)$$

with d the separation length. A charge of $\pm Q$ accumulates in both plates. The amount of charge per surface area or charge displacement is

$$D = \varepsilon_0 E, \qquad (2)$$

with ε_0 the dielectric permittivity of free space. When the vacuum is replaced by a dielectric medium then ε_0 is increased to the permittivitiy $\varepsilon_{\mathrm{di}}$ of this dielectric. This value is commonly referred to as the relative permittivity or dielectric constant

$$k = \frac{\varepsilon_{di}}{\varepsilon_0}. \qquad (3)$$

If we consider a constant E then it can be seen from Equation 2 that the effect of introducing a dielectric is that D increases. This is because the dielectric, in response to the applied field, polarizes in the opposite direction of the applied field which counteracts the applied electric field so that an additional amount of charge accumulates in the electrodes in order to maintain the same electric field. The explanation for this opposite effect can be envisaged by noting that a positive charge in the metal electrode will attract a negative charge in the dielectric through Coulomb attraction. For a ferroelectric capacitor, Equation 2 becomes

$$D = \varepsilon_{di} E + P, \qquad (4)$$

with an additional polarization P. This polarization arises due to internal dipole moments that can change their direction up or down, depending on the sign of an applied field. The macroscopic polarization P is determined by the size of the dipole moments, their orientation and their surface area density. Polarization P is hysteretic, which means that it does not depend on the instantaneous applied field, but on the history of the applied field. This behaviour can be described by the Preisach model, which consists of an ensemble of

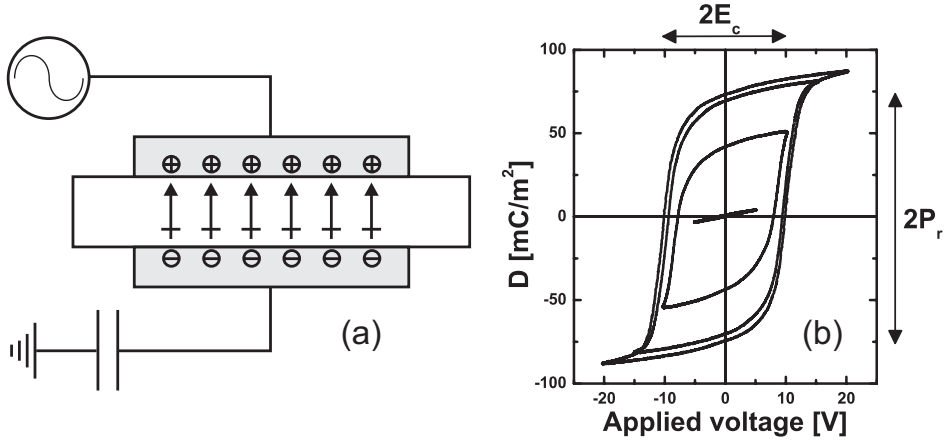

Figure 1 a, Sawyer-Tower circuit in which a sinusoidal voltage signal is applied to a ferroelectric capacitor. The displacement charge is measured using the voltage buildup on a reference capacitor that is connected in series. The voltage drop over the reference capacitor is minimized by using a large reference capacitor. **b**, Displacement D vs. applied voltage V hysteresis loop measurements using a Sawyer-Tower circuit. Scanning voltage levels of 5 V, 10 V, 15 V and 20 V are included to show that the ferroelectric polarization first appears and then saturates.

individual hysteretic elements [3]. At high applied fields, polarization P saturates because the finite number of dipole moments are all aligned. The remanent polarization P_r and the coercive field E_c are measured in the saturated regime.

A standard method for measuring P_r and E_c is with a Sawyer-Tower circuit [4], which is illustrated in Figure 1a. A sinusoidal voltage signal is applied to one of the electrodes of the ferroelectric capacitor and the amount of charge displacement in the other electrode is measured using the voltage it creates over a reference capacitor connected in series. A typical measurement result is depicted in Figure 1b. At a low voltage level of 5 V, only a linear component is measured. Evidently, the electric field is not high enough to affect P. A hysteretic response starts to appear at 10 V and between 15 and 20 V the signal saturates. As indicated in Figure 1b, the total height of the saturated loop at zero field is $2P_r$ and the total width of the loop at zero displacement charge D is $2E_c$.

iii. Ferroelectricity in P(VDF-TrFE) thin film capacitors

Poly(vinylidene fluoride-trifluoroethylene) (P(VDF-TrFE)) is a copolymer of polyvinylidene fluoride (PVDF) and polytrifluoroethylene (PTrFE). Its molecular formula is presented in Figure 2. PVDF is produced on an industrial scale and sold with brandnames such as Solef and Kynar. One of the main applications is as a protection coating, due to its abrasion resistance, stiffness, nonflammability, high chemical stability and radiation tolerance. It can be processed from the melt to get any shape required. When cooled from the melt, the crystalline phase in this semicrystalline material attains the α polymorph in which the polymer chain its stereochemical conformation is alternatingly trans and gauche [5]. With operations such as annealing, poling and film stretching one can obtain at least 4 different polymorphs. The most interesting polymorph in the present context is the β polymorph in which the chain conformation is all-trans. This is because the β polymorph has the highest ferroelectric response, due to an optimal alignment of all the dipole

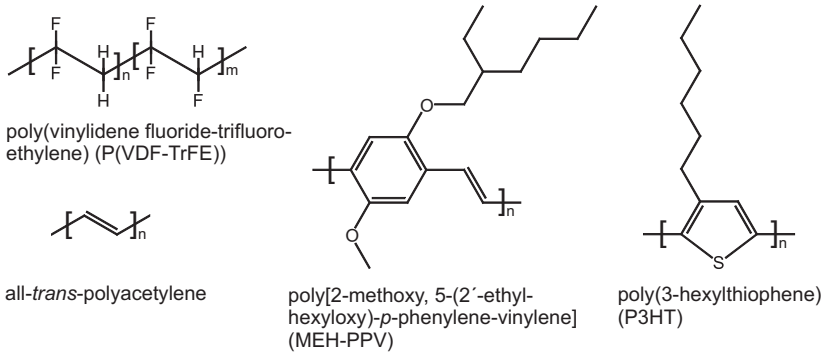

Figure 2 Chemical formulas and names of several molecules. Abbreviated names are included in parentheses.

moments in the crystal unit cell. These dipoles extend from the electronegative fluoride atoms to the slightly electropositive hydrogen atoms perpendicular to the polymer chain direction.

In order to obtain the β polymorph directly from solution, PVDF is copolymerized with PTrFE. This is said to enhance the all-trans conformation associated with the β polymorph because PTrFE has three fluoride atoms per monomer, which are larger than hydrogen and therefore induce a stronger steric hindrance. The ferroelectric phase is obtained for molar ratios between 50 and 80 % of PVDF [6]. The solution-processability enables the use of spin coating and other techniques to produce ferroelectric polymer films. The P(VDF-TrFE) films used for this thesis were all spin coated, as illustrated in Figure 3. A solution is deposited onto the substrate, which is then spun around at a high speed so that the solution is spread out by the centrifugal force. Excess solution flies off the substrate and simultaneously, some of the solvent evaporates. The evaporation process raises the concentration and the viscosity of the remaining solution. This high viscosity prevents the solution from exiting the substrate and a thin film of solution remains. Continued spinning evaporates the rest of the solvent after which a thin film of polymer is obtained. Spin coating is a widely used technique in the semiconductor industry for the deposition of polymer resist layers which take part in the lithographic patterning process.

Figure 4 illustrates the ferroelectric switching mechanism in P(VDF-TrFE). The dipole moment direction is changed by a rotation of the molecule. This rotation is facilitated by the single carbon-carbon bonds that allow for some flexibility. The switching

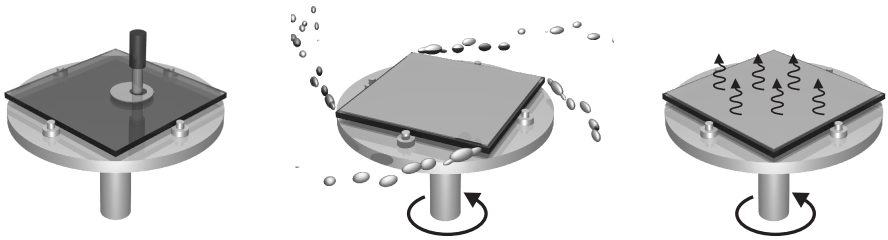

Figure 3 Illustration of the spin coating technique. A solution containing a polymer is deposited on a substrate, which is then spun round at a high speed. Excess solution flies away and the solvent evaporates, leaving a polymer film behind.

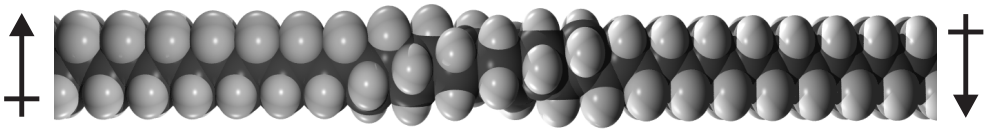

Figure 4 Artistic impression of how a ferroelectric switching event may occur in P(VDF-TrFE). On the left, the carbon backbone has the larger fluoride atoms on top and the smaller hydrogen atoms below. The molecule is turned upside down on the right by a gradual rotation.

time depends on the applied field strength E according to

$$t_{sw} = t_{\infty}\ e^{E_a(T)/E}, \qquad (5)$$

with an activation field E_a of 0.85 GV/m and t_{∞} the switching time at infinite field of 10 ns [7]. t_{sw} is defined here as the time between the start of an applied voltage pulse and a peak maximum of $\partial D/\partial\log(t)$. The switching process occurs by nucleation of small reversed domains followed by domain growth. The time limiting factor for switching in P(VDF-TrFE) is the nucleation process, regardless of the applied field. The nucleation process is thermally activated, which is represented in Equation 5 by the temperature dependence of E_a. Consequently, the switching time increases with decreasing temperature. The coercive field E_c arises from Equation 5 through the exponential decrease of the switching time with increasing field. At a field of 30 MV/m, the switching time is 6 hours, which is much longer than any normal measurement timescale and therefore not noticeable. At one particular field the switching time will become fast enough. This is at around the coercive field of 50 MV/m in P(VDF-TrFE).

If one compares the properties of P(VDF-TrFE) to the inorganic ferroelectric PZT, then the most important differences are that the coercive field is higher, the remanent polarization is lower, the switching time is longer and the required annealing temperature is lower. The low annealing temperature is advantageous because it makes it easier to combine the material with other materials and processes. Another important difference is that the material is a wide bandgap insulator, while PZT is usually semiconductive due to imperfections created during crystal growth. Besides P(VDF-TrFE) there are also nylon-based and other ferroelectric polymers, but they mostly have a lower performance. The switching time of ferroelectric nylons for example, is known to be longer by four orders of magnitude than that of P(VDF-TrFE) at the same applied field [5].

P(VDF-TrFE) is the only known ferroelectric polymer that has a measurable Curie temperature T_C which marks a transition from a ferroelectric to a paraelectric phase. The T_C increases with increasing VDF content from 70 °C at 50 mol% to 140 °C at 80 mol%. Pure PVDF has a T_C that is above its melting temperature, so this transition is not accessible with experiments. At the Curie transition, the crystal structure has an order-disorder type transition. The disorder is introduced in the conformation of the molecules, which take on a random mixture of trans and gauche combinations [6]. The material becomes paraelectric because the sum of a randomly distributed dipole moment direction is zero.

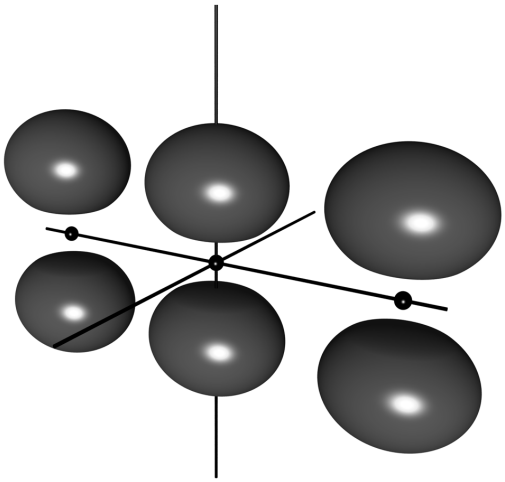

Figure 5 Three twin lobes that represent the approximate shape of p-orbitals. They are aligned in the vertical direction.

iv. Conjugated polymer semiconductors

A conjugated polymer has a carbon atom backbone in which there is an alternation of single and double bonds, as illustrated with the molecule all-*trans*-polyacetylene in Figure 2. Metallic-like electronic conduction in the conjugated polymer polyacetylene was first reported in 1977 [8]. This discovery was awarded with a Nobel prize in the year 2000 because conjugated polymers became an important scientific field in terms of practical applications and interdisciplinary development between chemistry and physics. Some applications for metallic-like conjugated polymers are corrosion protection, electromagnetic shielding and printable interconnects. Conjugated polymer semiconductors are being used for lighting applications and flexible integrated circuits. It is an interdisciplinary field because the physical properties of conjugated polymers can be tailored by altering their chemical structure and by electrochemical doping.

The carbon atom in its ground state has an electron configuration of $1s^2\ 2s^2\ 2p^2$, so of the valence orbitals, the 2s orbital is filled and two out of three p orbitals are half-filled. The presence of two unpaired electrons would suggest that carbon normally forms two chemical bonds. However, carbon usually forms four bonds and this can be explained by a concept called promotion. For carbon, it is energetically favourable to promote one 2s electron to the third unfilled 2p orbital to create four half-filled orbitals because it enables the ability to form four chemical bonds. The energy investment required is less than what is obtained by the increased number of bonds. The way that carbon bonds to other atoms is often described using the concept of hybridization. The idea is that the four half-filled orbitals created by the promotion can form new hybrid orbitals that are linear combinations of the participating atomic orbitals. For example, the hybridization state sp^3 implies that the four atomic orbitals form four hybrid orbitals. These hybrid orbitals can form bonds by combining with orbitals on another atom. Examples of compounds with sp^3 hybridized carbon are simple alkanes such as methane (CH_4) and polyethylene ($(CH_2CH_2)_n$). Alkane

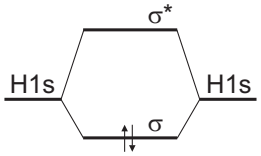

Figure 6 Molecular orbital energy-level diagram of H_2. The two H1s orbital levels on either side of the figure combine into the bonding orbital σ and the antibonding orbital σ* in the middle. The bonding orbital is occupied by two electrons.

polymers such as polyethylene are usually good insulators, i.e. they conduct very little current even at high electric fields.

The hybridization state of the alternatingly single and double bonded carbon atoms in conjugated molecules is sp^2. In this hybridization state, one s orbital and two p orbitals form three hybrid orbitals and one p orbital is left over. The three hybrid orbitals form σ bonds, two with neighbouring carbon atoms and one with a third atom. They are called σ bonds because their symmetry resembles that of an s orbital (they have cylindrical symmetry along the bond direction). The left over p orbitals can combine to form π orbitals, which have a symmetry that resembles that of p orbitals. The shape of these p orbitals is illustrated in Figure 5. The fact that the lobes extend perpendicular to the chain direction promotes a planar chain conformation because this gives the highest p orbital overlap. The π orbitals have a delocalized character, which means that the electrons that occupy these orbitals are shared throughout the whole molecule. The consequences of this delocalization can be illustrated using Hückel theory.

Hückel theory

This theory is actually a set of approximations in the framework of molecular orbital (MO) theory that apply specifically to conjugated molecules [9]. MO theory describes the structure of the electron orbitals in molecules as linear combinations of the atomic orbitals. For example, a MO of H_2 that originates from the same 1s atomic orbital ψ_{1s} on two hydrogen atoms A and B can be written as

$$\psi = N\left(\psi_{1s,A} + \psi_{1s,B}\right), \qquad (6)$$

with N a normalization factor. This orbital is a bonding orbital, which means that occupying the orbital lowers the energy of the molecule relative to the energy of the separated atoms. The number of atomic and molecular orbitals should be equal, so H_2 must have a second MO. This MO is

$$\psi' = N\left(\psi_{1s,A} - \psi_{1s,B}\right), \qquad (7)$$

which is an antibonding orbital; occupying it increases the energy of the molecule. This is partly due to the fact that an antibonding electron is absent in the internuclear region and does not shield the electrostatic repulsion of the atom cores. In Figure 6 we present the molecular orbital energy-level diagram of H_2. The two H1s orbitals combine to form a bonding σ orbital and an antibonding σ* orbital. The neutral molecule has two electrons at

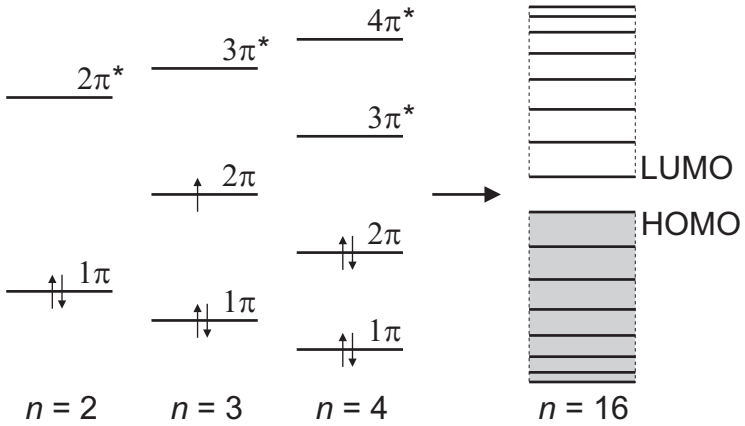

Figure 7 Molecular orbital energy-level diagrams derived from Hückel theory of linear conjugated alkenes (ethene, propene, butadiene) with *n* the number of carbon atoms in the molecule. The π* orbitals are antibonding. For *n* = 16 the lower half of orbitals are occupied in the ground-state, which is indicated by the gray rectangle.

its disposal, which fill the lower orbital in accordance with the Pauli exclusion principle: a maximum of 2 electrons per orbital, with antiparallel spin orientation. He_2 has the same diagram but it has two extra electrons at its disposal, which fill the antibonding orbital. The energy increase from filling the antibonding orbital more than negates the energy decrease from filling the bonding orbitals. This explains why He_2 is not a stable molecule.

Hückel theory considers the π bonds as being completely separate from the σ bonds and the σ bonds are considered as fixed. For the smallest possible conjugated molecule ethene (CH_2=CH_2), this means that we only need to consider the two C2p orbitals. Similar to the above discussion, these two orbitals form a bonding and an antibonding orbital and because there are two electrons available, only the bonding orbital is filled. Hence, ethene is a stable molecule. The energy levels of these orbitals can be calculated by finding a set of coefficients to linearly combine the atomic orbitals in a way that has the minimal energy. With the approximations of Hückel theory, this can be done by solving a relatively simple secular determinant. It is also quite easy to extend the calculation to a conjugated polymer with an arbitrary length [10]. The results are illustrated in Figure 7. On the left, we see the bonding and antibonding orbitals of ethene. As the chain length of the molecule is increased from left to right, one observes an increase of the spread of the energy levels. This spread is limited by a resonance integral, which depends on the amount of overlap between the atomic orbitals. If we keep on increasing the chain length, the effect of this limitation is that the energy levels approach each other. One can imagine that this will eventually lead to the formation of an energy band, as illustrated on the right side in Figure 7 where the energy-level diagram for a chain length of 16 is depicted. In the lowest energy configuration, the lower half set of orbitals is filled and the upper half is unfilled. This energy band diagram is similar to the valence and conductance band diagram that is familiar to us from descriptions of other semiconductors. The emergence of energy bands allows us to use the classical description of a semiconductor. However, Hückel theory erroneously predicts that the bandgap becomes insignificantly small as the polymer chain length becomes larger. The bandgap is defined by the energy difference between the highest-occupied-molecular orbital (HOMO) and the lowest-unoccuppied-molecular-orbital

(LUMO). Optical absorption experiments have shown that the bandgap indeed decreases in the series ethene, butadiene, hexatriene, but not in the way predicted by theory: At some point, longer conjugation does not decrease the bandgap anymore [11]. This convergence is also confirmed by more advanced theoretical predictions. This shows that conjugated polymers are intrinsically semiconductors.

One can change the semiconducting properties by changing the chemical nature of the conjugated polymer, for example by incorporating cyclic conjugated systems into the carbon backbone. One can also increase the charge carrier doping level by oxidizing the polymers with halogen gases or by other electrochemical means. The metallic-like conduction in polyacetylene mentioned above was obtained with halogen gases. The halogen molecule removes an electron from a polymer chain to create an immobile negatively charged halogen ion and a mobile positive charge on the polymer chain.

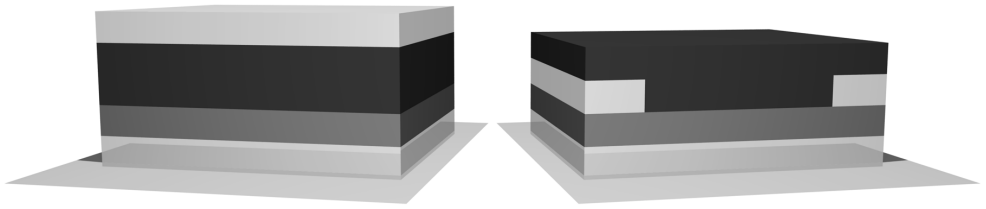

Figure 8 General device structure of a metal-insulator-semiconductor (MIS) diode (left) and a field-effect transistor (FET, right). Both structures have a gate electrode below, then an insulator layer, followed by a semiconductor layer. The MIS diode has a semiconductor contact electrode on top. The FET has two semiconductor contacts called source and drain. The area in between these electrodes is called the semiconductor channel.

v. Metal-insulator-semiconductor diodes and field-effect transistors

Here we introduce two device structures and in the next section we apply them to conjugated polymers. If one replaces an electrode plate of a capacitor with a semiconductor layer then the charge displacement described by Equation 2 will be induced in a semiconductor. To do this, one does need to apply electrode contacts to the semiconductor to transport the charge in and out of the semiconductor. Two structures of this kind are depicted in Figure 8: a metal-insulator-semiconductor (MIS) diode and a field-effect transistor (FET). Both devices have a gate electrode below an insulator layer that separates it from a semiconductor layer. The MIS diode has one semiconductor contact electrode, but the FET has two semiconductor contacts called source and drain. The area in between the source and drain near the insulator is called the semiconductor channel. Both structures are widely used in the semiconductor industry. MIS diodes are the active devices in CCD cameras and FETs are the basis for the integrated logic circuits in today's computer chips. The FETs in computer chips are a bit more complicated than depicted here, but the basic working mechanisms are the same.

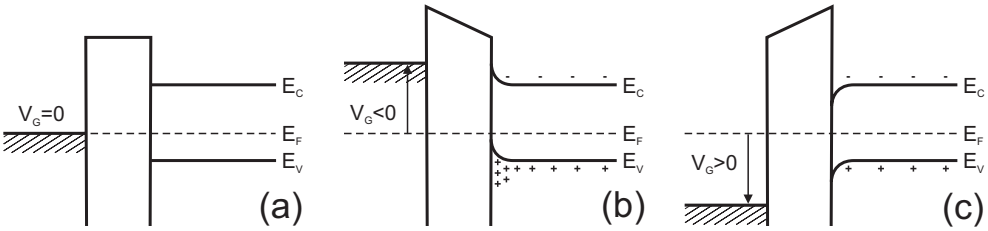

Figure 9 Energy-band diagrams of a metal-insulator-semiconductor structure at several gate voltages. The semiconductor is p-type. E_V, E_F and E_C indicate the energy levels of the top of the valence band, the Fermi energy and the bottom of the conduction band, respectively. **a**, At zero gate voltage the energy bands of the semiconductor are in their intrinsic state. **b**, A negative gate voltage bends the energy bands of the semiconductor upwards, which results in hole accumulation. **c**, A positive gate voltage bends the bands downwards and depletes the semiconductor.

We will briefly examine the functionality of MIS diodes and FETs. The presented examples focus on a semiconductor that is unintentionally doped and p-type because this is the most relevant case for this thesis [12,13]. In order for the devices to work as intended, one first of all needs adequate charge transport between the semiconductor contacts and the semiconductor, i.e. the transport across the interface should not be limited by a Schottky barrier. A Schottky barrier can arise in the following way: When the metal and semiconductor are brought into contact their Fermi energy levels will align. The Fermi energy is the energy up to which the energy bands of a material are occupied. At zero temperature, it is equal to the top of the valence band, but it is higher at nonzero temperatures. If the two materials have unequal Fermi energy levels, the Fermi energy leveling will result in a charge flow across the interface. This can result in the formation of a region with a depletion and/or accumulation of holes and electrons in the semiconductor near the interface, which can hinder the flow of either holes or electrons across the interface. We therefore assume that the metal work function is equal to or higher than that of the p-type semiconductor, to avoid this problem. In other words, we assume that current is limited by the semiconductor bulk, not by charge injection. In this situation, the metal electrode is called an Ohmic contact.

Figure 9 presents energy-band diagrams for a metal-insulator-semiconductor structure at three different gate bias conditions. The semiconductor contact can be disregarded assuming that it is Ohmic. Figure 9a presents the situation when the voltage difference applied to the gate electrode and the semiconductor contact is zero. We assume that the Fermi energies of the gate electrode and the semiconductor contact are about the same, so that the semiconductor energy bands are in their intrinsic state. An applied gate bias can stabilize or destabilize the occupation of states within the bandgap. Consequently, the conduction and valence band will bend either up- or downwards at the semiconductor-insulator interface, depending on the sign of the applied gate bias. In Figure 9b, a negative bias is shown to bend the bands upwards. Because this brings the valence band closer to the Fermi energy level, positive charge carriers accumulate at the semiconductor-insulator interface. The conduction band on the other hand, is bended further away from the Fermi level which leads to electron depletion. In Figure 9c, a positive gate bias bends the bands downwards, which depletes the interface of positive charge carriers. The downward bending of the conduction band does not lead to an appreciable electron accumulation

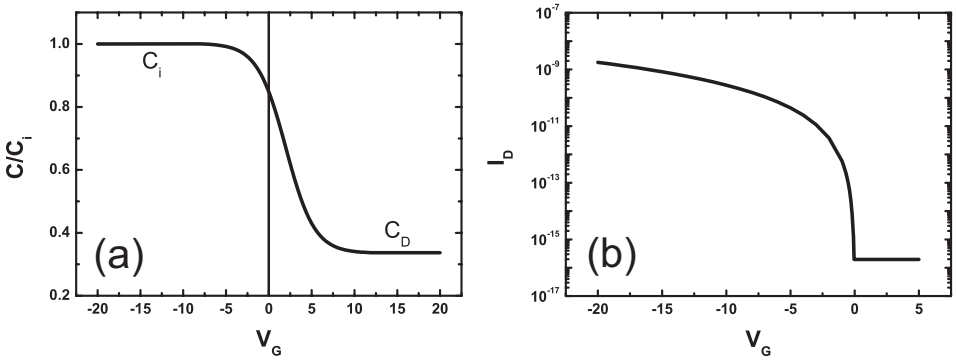

Figure 10 a, Example capacitance-voltage measurement on a MIS diode. C is the device capacitance and V_G is the gate voltage. The vertical scale is divided by the insulator capacitance C_i. **b**, Example transfer curve measurement on a FET which represents the gate voltage dependence of drain current I_D.

because the distance to the Fermi energy remains large. The available electrons do not have enough energy to occupy the newly formed states.

Having established the gate field-effect induced band bending in a semiconductor, we now qualitatively evaluate its effects in measurements. Figure 10 presents two examples of measurements on MIS diodes and FETs. Figure 10a depicts the gate voltage dependence of the MIS diode capacitance. The maximum capacitance is obtained at negative gate voltages and is equal to the insulator capacitance C_i. As the gate voltage is brought from the negative to the positive and the semiconductor becomes partially depleted, the depletion layer acts as a capacitance in series with the insulator. The minimum capacitance is obtained when the semiconductor layer is fully depleted. This capacitance value is determined by the layer thicknesses and dielectric constants of the insulator and semiconductor layers. Obviously, the most interesting part of this curve is in between full depletion and accumulation. One can apply a so-called Mott-Schottky analysis to derive several properties of the semiconductor such as the doping density (the number of mobile charge carriers per unit of volume). The derived information is complementary to the information that can be derived from FET measurements, which makes the MIS diode a valuable analytical tool.

Figure 10b presents a transfer curve measurement on a FET. This measurement represents the gate voltage dependence of the current that results from applying a fixed voltage difference between the source and the drain. The current response reflects the charge carrier accumulation and depletion in response to the gate bias. At negative gate bias, the accumulation induces a high drain current and at positive gate bias, the current becomes essentially zero. One can compare the working mechanism of a FET with a valve: the gate electrode is a tap that controls the current flow between source and drain. The drain voltage used here is small compared to the gate voltage so that the charge carrier accumulation is uniform along the semiconductor channel. Consequently, the drain current scales linearly with the drain voltage, just like a normal resistor. The drain current saturates at high drain biases because this bias counteracts the gate bias locally at one of the semiconductor contacts.

The strength of the field-effect exerted by the gate bias is a product of the gate bias V_G and the gate insulator capacitance per unit area C_i. This product is an amount of charge per unit area, or charge displacement D. An important semiconductor material parameter is the mobility, which corresponds to the ease with which the charge carriers move under the influence of an applied field. In the linear regime, this parameter can be derived in the following way: If we increase the gate bias V_G with a small amount δV_G, then D will increase by $C_i \delta V_G$. And if the additional charge carriers have a mobility μ then the drain current will increase by

$$\delta I_D = \frac{W}{L} \mu C_i V_D \delta V_G , \qquad (8)$$

with W and L the width and length of the semiconductor channel, respectively. It follows that the mobility can be derived from the slope of the transfer curve using

$$\mu = \left(\frac{L}{W C_i V_D} \right) \left. \frac{\partial I_D}{\partial V_G} \right|_{V_D \to 0} . \qquad (9)$$

For logic circuit applications, FETs should have a high mobility so that they can be switched on and off as fast as possible. However, a more important parameter is the transconductance which is the product of the mobility and the gate dielectric capacitance. The transconductance is essentially the amplification factor of the transistor. The higher this value, the more effect a given gate voltage change will have on the drain current.

vi. Conjugated polymer based field-effect transistors

The first report on a conjugated polymer based FET was published in 1986 and used a polythiophene as the semiconductor layer, a SiO_2 gate insulator layer and gold contacts [14]. Gold contacts are often used for polymer based FETs because its workfunction of around 5 eV creates an Ohmic contact with conjugated polymers such as polythiophene since they typically have an ionization potential of around 5 eV. The transistor measurements were performed in vacuum because conjugated polymers can be affected by atmospheric conditions; they either photo-oxidize or reach a higher doping level. The reported field-effect mobility for holes was in the range of ~10^{-5} cm^2/Vs. As a comparison, pure silicon has a hole mobility of 450 cm^2/Vs [12]. The extremely low mobility was attributed to the fact that the polythiophene is an amorphous material with a very low doping level. The next section discusses this issue further.

The mobility is not only affected by the properties of the conjugated polymers. It has been shown that the gate insulator-semiconductor interface is another important factor. An interface roughness higher than ~1 nm can drastically reduce the mobility due to charge carrier trapping, according to several reports [15,16]. Insulator layers with a high dielectric constant can negatively affect the mobility because they usually have randomly oriented dipole moments near the interface, which increase the energetic disorder inside the semiconductor [17]. The importance of the gate insulator is most evident for n-type

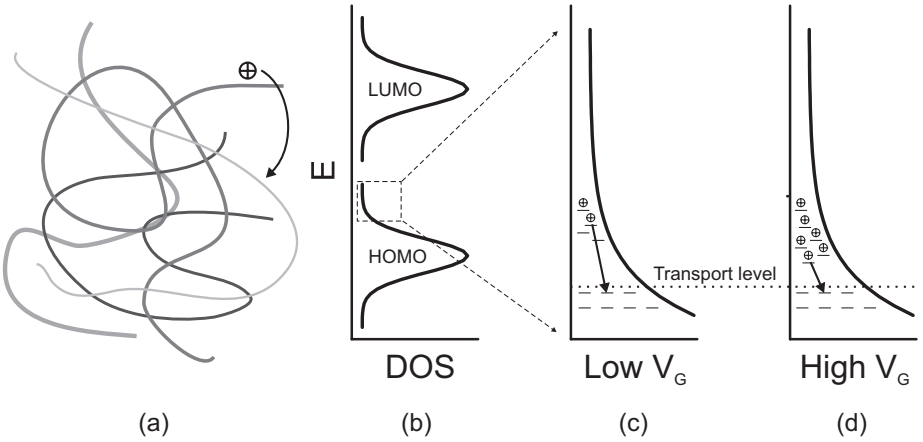

Figure 11 a, A random mesh of polymer chains in which charge carriers hop between localized states. **b**, The HOMO and LUMO levels of the localized states have a Gaussian distribution. **c**, Transport occurs in the upper tail of HOMO. The shape is approximated by an exponential. Here the gate voltage and the charge carrier density is low, which means that the energy barrier for hopping transport is relatively high. **d**, A high gate voltage and charge carrier density lowers the energy barrier for hopping transport.

conduction in conjugated polymers. A general observation of this type of conduction has only recently been achieved with a specific choice for an insulator material [18].

Vissenberg model

One of the most successful models that describe the charge transport in disordered organic transistors quantitatively is the Vissenberg model [19]. It is based on the premise that the charge carriers occupy and hop between localized states with a temperature-activated hopping process. The physical origin of this behaviour is addressed in the following discussion. There is ample evidence that on a molecular scale, charge transport in conjugated polymers is polaron-based [20]. Polarons are charge carriers that are localized on a polymer chain and whose charge deforms the local molecular conformation. The interaction of polarons with the molecule is one step towards explaining why the mobility in conjugated molecules is much lower than in silicon, where the charge carriers are essentially free to move around. However, the mobility is not limited by polaron mobility in a molecule but by intramolecular charge transport. The electronic overlap between polymer chains is very limited, because conjugated polymer materials generally have a high degree of disorder. The disorder is facilitated by the weak van der Waals interactions that hold the materials together. The net effect of the disorder is that the charge carriers occupy localized states between which they need to hop. The localization may be further enhanced by kinks, twists or chemical defects along the polymer chain which interrupt its conjugation. Because the hopping process is the limiting factor, the charge transport can be described by considering only this part of the transport conveyor belt.

Figure 11a illustrates the envisioned hopping process. The disordered polymer chains form a spaghetti-like mesh which creates a discontinuous energy landscape for a charge carrier. The localized states are expected to have a distribution of states with

different energies. This distribution or density of states (DOS) is usually approximated by a Gaussian, as presented in Figure 11b. Hole transport is expected to occur in the upper tail of the Gaussian DOS of the HOMO level. In the Vissenberg model, the shape of this tail is approximated by an exponential DOS, like in Figure 11c and d. The model describes the transport as equivalent to transport through a resistor network where the nodes of the network have different energies according to the exponential DOS [21]. The percolation criterion through the network is then related to the temperature, the position of the Fermi level, and the width of the exponential tail of the DOS. The particular type of hopping used in the model is called variable-range hopping, which means that a carrier can either hop a small distance with a high activation energy or hop over a long distance with a low activation energy. One of the most important consequences of the model is that the effective charge carrier mobility increases with increasing charge density, i.e. the mobility is gate voltage dependent. This is because the additional charges on average occupy higher energy sites and therefore require less energy for hopping transport. This effect is illustrated in Figure 11d.

The formula that is eventually derived describes the drain current dependence on gate voltage and temperature as

$$I_D = \frac{WV_D\varepsilon_0\varepsilon_r\sigma_0}{Le}\left(\frac{T}{2T_0 - T}\right) \times \sqrt{\frac{2k_bT_0}{\varepsilon_0\varepsilon_r}}\left[\frac{\left(\frac{T_0}{T}\right)^4 \sin\left(\pi\frac{T}{T_0}\right)}{(2\alpha)^3 B_c}\right]^{\frac{T_0}{T}} \times \left\{\sqrt{\frac{\varepsilon_0\varepsilon_r}{2k_bT_0}}\left[\frac{C_i(V_G - V_{so})}{\varepsilon_0\varepsilon_r}\right]\right\}^{\frac{2T_0}{T}-1}, \quad (10)$$

with L and W the length and width of the channel, V_D the drain voltage, $\varepsilon_0\varepsilon_r$ the dielectric constant of the semiconductor, e the elementary charge, k_B the Boltzmann constant, T_0 the width of the exponential density of states for holes, B_c a critical number for the onset of a percolating conduction path of 2.8, α^{-1} the effective overlap parameter between localized states, C_i the insulator capacitance per unit area and V_{so} the switch-on voltage [22]. The parameters can be determined experimentally by fitting the formula to transfer curves that were measured at several different temperatures.

Conjugated polymers used for this thesis

Figure 2 presents the chemical structures of the conjugated polymers poly[2-methoxy, 5-(2´-ethyl-hexyloxy)-*p*-phenylene-vinylene] (MEH-PPV) and poly(3-hexylthiophene) (P3HT), that were used for this thesis. MEH-PPV is a PPV derivative that is often used for polymer light-emitting diode (PLED) applications. The first report on PLEDs in 1990 used a PPV [23]. These PLEDs are currently starting to be sold commercially, integrated in a variety of products. MEH-PPV has been tailored for solution-processabilty. The sidechains

of the molecule facilitate its solubility in toluene, which has advantageous film-forming properties during spin coating. MEH-PPV is amorphous and has a field-effect mobility of around $5 \cdot 10^{-4}$ cm^2/Vs at room temperature. A higher mobility of up to 0.3 cm^2/Vs can be obtained in P3HT [24]. This enhancement was enabled by the synthesis of regioregular poly(3-hexylthiophene), which enhances the crystallinity of the material [25]. Regioregularity means that the monomers are linked head-to-tail up to a high degree, where the head and tail are the left and right side of the monomer which differ by the presence of an alkane sidechain. Detailed studies have shown that the polymer chains self-organize in stacked lamellae, which significantly enhances interchain charge transport [26].

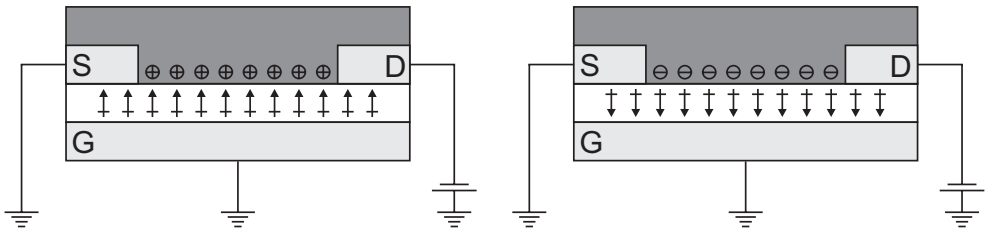

Figure 12 Method for information read-out of a ferroelectric field-effect transistor. The polarization state of the gate dielectric attracts either holes or electrons to the semiconductor interface, which attenuates the current measured by applying a voltage difference between the source and drain electrodes. S, D and G are the source, drain and gate electrodes, respectively.

vii. Ferroelectric field-effect transistors

Having introduced all the different components, we now proceed to put them together and introduce the ferroelectric field-effect transistor (FeFET), which is simply a field-effect transistor with a ferroelectric gate insulator. Figure 12 illustrates how these devices are supposed to work. The ferroelectric polarization of the gate dielectric should attract either holes or electrons in the semiconductor in a remanent way. Due to a difference in hole and electron mobility, this then attenuates the conductance of the semiconductor channel. A small drain voltage can then be used to probe the conductance without affecting the polarization state of the gate dielectric. The FeFET was introduced in 1966, using triglycine sulfate (TGS) as the ferroelectric material and tellurium as the semiconductor [27]. The suggested applications were not only as a memory device, but also as a latch transistor (as opposed to the valve-like characteristics of normal transistors) and as an electrically variable resistor.

At first glance, building a FeFET may seem a bit superfluous because the ferroelectric layer itself has a hysteretic polarization which can be used for nonvolatile memory applications. One can indeed use the capacitor depicted in Figure 1a for this purpose, but this approach has several disadvantages. Two major disadvantages are degradation and scaling. The degradation problem is associated with the read-out operation for a ferroelectric capacitor. It consists of applying a field and measuring the displacement response that is either high or low, depending on the initial polarization direction. If the response is high then the previously stored orientation needs to be restored with a second programming operation. This kind of a read-out operation, which can affect the stored

information, is called a destructive read-out. An important disadvantage of this method is that the number of programming cycles during the normal lifetime of the device is enormous. The industrial standard is 10^{12} cycles. Unfortunately, ferroelectric capacitors degrade when they are programmed many times. An important type of degradation is called fatigue, which means that the amount of ferroelectric polarization decreases with the number of programming cycles. The decrease makes it harder to sense the displacement charge response during the read operation and eventually makes it impossible. FeFETs have a nondestructive read-out operation, which lowers the programming cycle standard from 10^{12} to 10^5, which alleviates any degradation issues.

The second major disadvantage of using ferroelectric capacitors is their scaling behaviour. Reduction of the capacitor area is highly desirable because it increases the memory density. The average current during a ferroelectric switching event scales with remanent polarization P_r, capacitor area A and ferroelectric switching time t_{sw} as

$$I \propto \frac{P_r A}{t_{sw}} . \qquad (11)$$

An area reduction therefore reduces the signal. By contrast, the drain current of a FeFET working in the linear regime scales with (using Equation 8)

$$I \propto \frac{W}{L} \mu V_D . \qquad (12)$$

It will also increase with the charge density in the semiconductor induced by the ferroelectric. Equation 12 shows that if L and W are reduced by the same factor, the read-out signal is unaffected by scaling.

There have been many efforts to make FeFETs with inorganic ferroelectric and semiconductor materials because of the envisioned advantages over many other nonvolatile memory technologies. Obtaining the envisioned performance has proven to be elusive however. There are several common problems, irrespective of the particular materials used. Generally speaking, these problems are attributed to two problems: Injection and subsequent trapping of charges in the ferroelectric and depolarization in response to a depolarization field [28,29]. Both effects can arise for a number of reasons. For example, to avoid charge injection into inorganic ferroelectrics one needs to add an insulator to separate the ferroelectric from the semiconductor. HfO_2 is a popular choice for this purpose. If the HfO_2 layer is too thin then one can imagine that this can lead to charge injection into the ferroelectric, which can then become trapped. These trapped charges will alter the way that the ferroelectric polarization affects the semiconductor channel conductance. If the HfO_2 layer is too thick then it creates a sizeable depolarization field onto the ferroelectric. This occurs due to the fact that the charges in the semiconductor have to compensate the ferroelectric polarization. Separating the two will result in ferroelectric depolarization. The depolarizing effect of incomplete compensation has been illustrated in a MIS diode with a semiconductor layer that had an insufficiently high density of negative charge carriers [30]. The ferroelectric polarized normally in hole accumulation mode, but the semiconductor was unable to provide charge carriers for the reverse polarization direction. Only an

extraordinarily large band bending in the semiconductor could provide the charge but this places a significant depolarization field onto the ferroelectric. A lack of polarization in the reverse direction was observed. By irradiating the semiconductor, additional charges were created, which resulted in ferroelectric polarization in both directions. With the irradiation method, effects other than band bending induced depolarization could be eliminated.

It is interesting to contemplate whether the problems described above are expected to apply to FeFETs made from P(VDF-TrFE) and conjugated polymers. Charge injection should not be a problem because P(VDF-TrFE) is a wide bandgap insulator, so there is no need for an additional insulator layer such as HfO_2. Insufficient charge compensation is expected to be a problem because conjugated polymers usually only provide positive charge carriers. However, as we will show in Chapter 2, the depolarization does not obstruct memory performance. High-performance solution-processed polymer FeFET nonvolatile memory elements were realized, while making sure that the ferroelectric effect is not masked by other effects such as charge trapping at the interface between the ferroelectric and semiconducting layers or by materials impurities. The effects of incomplete charge compensation are explored in Chapter 7.

viii. Short summaries of all chapters

Chapter 1

Due to the relatively high coercive field E_c of 50 MV/m of P(VDF-TrFE), sub-100 nm thick ferroelectric layers are required in order to attain an operation voltage below 10 Volts. Previous reports unfortunately observed a decline in the ferroelectric switching performance when the film thickness is reduced to less than 100 nm. Common observations are an increase of the coercive field, a lower remanent polarization and/or elongated switching time. In this Chapter we present the benefits of using a conductive polymer as opposed to aluminium for the bottom electrode. All aforementioned literature results were obtained on capacitors that had transition metal or aluminium bottom electrodes. Employing a polymer bottom electrode we demonstrate an almost unaffected remanent polarization, coercive field and switching time behaviour down to at least 65 nm This enables switching of nearly the full remanent polarization with only 5 V. This improvement enables the use of ferroelectric polymers in nonvolatile memories operating at a low voltage.

Chapter 2

In this Chapter we present high-performance solution-processed polymer FeFETs made from P(VDF-TrFE) and MEH-PPV as a semiconductor. Transfer curve measurements show that the drain current on/off ratio at zero gate voltage is 10^3 or higher, which is several orders of magnitude larger than previous state-of-the-art values. Identical FETs were prepared with polytrifluoroethylene (PTrFE) as the gate insulator. PTrFE is chemically and physically very similar to P(VDF-TrFE) but it is not ferroelectric. The similarity allowed us to use identical processing conditions for the nonferroelectric and ferroelectric FETs, which enables a direct comparison of the two devices. Transfer curve measurements on these FETs did not have an appreciable hysteresis. This ensures that the hysteresis observed for

the ferroelectric FETs is a ferroelectric effect and not due to any other unintended effect. The memory devices have a short programming time, long memory retention and high programming cycle endurance. Combined with the low-cost deposition method, this makes the device highly suitable for low-cost nonvolatile memory applications.

Chapter 3

Historically, organic FETs have worked mainly as unipolar p-type transistors, in which positive charges are accumulated in the channel by applying a negative gate voltage. As a result, the state-of-the-art integrated circuits based on organic FETs are based on unipolar p-type logic. From a performance point of view, however, ambipolar transistors are to be preferred. The advantages compared with unipolar logic are low power dissipation, higher operating frequencies, a good noise margin, and robust operation. Therefore, the transport of electrons and holes, the so-called ambipolar charge transport, in FETs is a highly desirable property. It is therefore an important question whether ambipolar organic semiconductors can be combined with a ferroelectricity-functionalized gate dielectric. We showed that in an ambipolar FeFET, the polarity of the channel can be remanently switched from p-type to n-type and back, depending on the polarization state of the ferroelectric. Due to the polarity switching, FeFETs are suited as a nonvolatile data-storage element in future logic circuits based on ambipolar organic FETs.

Chapter 4

The transistors used for Chapters 2 and 3 had a rather thick ferroelectric gate insulator layer. This results in a high programming voltage of 80 V or more. For practical applications this voltage needs to be as low as possible. Because ferroelectrics switch at a specific electric field, the coercive field, low-voltage operational FeFETs can be obtained by using a thin ferroelectric gate dielectric. In Chapter 4 we show that it is possible to obtain a programming voltage of 15 V. This operation voltage was achieved by optimizing the ferroelectric layer deposition technique using cyclohexanone as a spin-coating solvent, which results in thin, smooth and defect-free ferroelectric films. Previous publications on spin-coated P(VDF-TrFE) thin films used dimethylformamide or 2-butanone as solvents. These are good solvents, but they lack the high viscosity of cyclohexanone. It is also demonstrated that these thin-film FeFETs have a good data retention capability.

Chapter 5

In 2000 a pioneering work on capacitors with ultra-thin films of P(VDF-TrFE) and aluminium electrodes demonstrated the film thickness dependence of the coercive field E_c for thicknesses between 100 nm and 1 nm. With decreasing thickness, E_c first increases and then saturates below a thickness of 15 nm, to a value of 5 MV/cm. This increase and saturation of E_c was explained by a transition from extrinsic to intrinsic ferroelectric switching in the context of Landau-Ginzburg mean-field theory. An observed switching time elongation was also explained with the same theory. In 2005, new experimental results were reported that favour extrinsic switching and speak against intrinsic switching. But if intrinsic switching does not occur then why are the coercive field and the switching kinetics thickness dependent? In this Chapter we present the results of two published papers and new experimental results that support a lack of intrinsic switching and point to the

conclusion that the thickness dependence of the ultra-thin films is not a characteristic of P(VDF-TrFE) but a characteristic of the electrode interfaces.

Chapter 6

In organic FETs, most of the charge carriers travel within a distance of about 2 nm from the interface with the gate insulator. If this interface is rough on the scale of nanometers or more, then one can imagine that these roughness valleys and hills will obstruct the flow of charge carriers. This brings us to a problem: The top surfaces of spin-coated P(VDF-TrFE) films are quite rough. One solution to this problem is to use a smoothing layer between the ferroelectric and the semiconductor. For memory devices however, this is not a usable solution because this buffer layer suppresses the effects from the ferroelectric polarization of the gate dielectric. In Chapter 6 we present work that solved the problem by another method: Instead of depositing the semiconductor on top of the ferroelectric, as in Chapters 2 to 4, we deposit the ferroelectric on top of the semiconductor. The reason that this works is because we can spin-coat the semiconductor in such a way that is has a low top surface roughness, which can not be done with P(VDF-TrFE). It was shown that the new method increases the charge transport mobility of regioregular poly(3-hexylthiophene) by a factor of 10.

Chapter 7

In this Chapter we present metal-insulator-semiconductor (MIS) diodes. We use the unique capabilities of MIS diodes to answer two important questions about the measurements on FeFETs presented in Chapter 2, 4 and 6. First, what happens to the ferroelectric polarization state of the gate dielectric after depleting the semiconductor with a positive gate voltage? It is feasible that the ferroelectric keeps the semiconductor depleted, but it is also possible that the ferroelectric depolarizes due to the lack of free (minority) charge carriers that compensate the ferroelectric polarization charge. Capacitance-voltage measurements on MIS diodes show that a remanent depletion of charge carriers does not occur at the ferroelectric-semiconductor interface after a programming operation towards depletion. This result indicates that unipolar polymer FeFETs have a drain current bistability at zero gate bias because they are either in a state where the ferroelectric attracts charge carriers in the semiconductor, or in a depolarized state. Secondly, what is the surface charge density induced by the ferroelectric polarization in the on-state of the FeFETs? The value was estimated using an indirect method in Chapter 2 and 6. Here we report a direct measurement of the amount of charge that enters and leaves the semiconductor-insulator interface. The amount of remanent charge induced by the ferroelectric is significantly larger than the previous value.

References

[1] J. Valasek, Physical Review 1922, 19, 478.

[2] L.E. Cross, R.E. Newnham, *History of ferroelectrics in Ceramics and Civilization Vol. III* 1987, The American Ceramic Society, Ohio. A download is available at www.ieee-uffc.org/femain.asp?page=e003

[3] I.D. Mayergoyz, *Mathematical models of hysteresis* 1991, Springer-Verlag, New York.
[4] C.B. Sawyer, C.H. Tower, Physical Review 1930, 35, 269.
[5] H.S. Nalwa, ed. *Ferroelectric polymers*. 1995, Marcel Dekker, Inc.: New York.
[6] T. Furukawa, Phase Transitions 1989, 18, 143.
[7] T. Furukawa, H. Matsuzaki, M. Shiina, Y. Tajitsu, Japanese Journal of Applied Physics 1985, 24, L661.
[8] H. Shirakawa, E.J. Louis, A.G. MacDiarmid, C.K. Chiang, A.J. Heeger, Journal of Chemical Society, Chemical Communications 1977, 579.
[9] P.W. Atkins, *Physical chemistry (5th ed.)* 1994, Oxford University Press, Oxford.
[10] R. Nix, *An Introduction to Molecular Orbital Theory*. 2002. A download is available at www.chem.qmul.ac.uk/software/download/mo/
[11] B. Nordén, E. Krutmeijer, *The Nobel Prize in Chemistry, 2000: Conductive polymers (Advanced Information)*, 2000.
[12] S.M. Sze, *Physics of semiconductor devices* 1981, Wiley, New York.
[13] A.R. Brown, C.P. Jarrett, D.M. de Leeuw, M. Matters, Synthetic Metals 1997, 88, 37.
[14] A. Tsumura, H. Koezuka, T. Ando, Applied Physics Letters 1986, 49, 1210.
[15] L.-L. Chua, P.K.H. Ho, H. Sirringhaus, R.H. Friend, Advanced Materials 2004, 16, 1609.
[16] S. Steudel, S. de Vusser, S. de Jonge, D. Janssen, S. Verlaak, J. Genoe, P. Heremans, Applied Physics Letters 2004, 85, 4400.
[17] J. Veres, S. Ogier, G. Lloyd, D.M. de Leeuw, Chemistry of Materials 2004, 16, 4543.
[18] L.-L. Chua, J. Zaumsell, J.-F. Chang, E.C.-W. Ou, P.K.-H. Ho, H. Sirringhaus, R.H. Friend, Nature 2005, 434, 194.
[19] M.C.J.M. Vissenberg, M. Matters, Physical Review B 1998, 57, 12964.
[20] H. Sirringhaus, Advanced Materials 2005, 17, 2411.
[21] A. Salleo, T.W. Chen, A.R. Völkel, Y. Wu, P. Liu, B.S. Ong, R.A. Street, Physical Review B 2004, 70, 115311.
[22] E.J. Meijer, C. Tanase, P.W.M. Blom, E.v. Veenendaal, B.-H. Huisman, D.M. de Leeuw, T.M. Klapwijk, Applied Physics Letters 2002, 80, 3838.
[23] J.H. Burroughes, D.D.C. Bradley, A.R. Brown, R.N. Marks, K. Mackay, R.H. Friend, P.L. Burns, A.B. Holmes, Nature 1990, 347, 539.
[24] D.H. Kim, Y.D. Park, Y. Jang, H. Yang, Y.H. Kim, J.I. Han, D.G. Moon, S. Park, T. Chang, C. Chang, M. Joo, C.Y. Ryu, K. Cho, Advanced Functional Materials 2005, 15, 77.
[25] Z. Bao, A. Dodabalapur, A.J. Lovinger, Applied Physics Letters 1996, 69, 4108.
[26] H. Sirringhaus, P.J. Brown, R.H. Friend, M.M. Nielsen, K. Bechgaard, B.M.W. Langeveld-Voss, A.J.H. Spiering, R.A.J. Janssen, E.W. Meijer, P. Herwig, D.M. de Leeuw, Nature 1999, 401, 685.
[27] P.M. Heyman, G.H. Heilmeier, Proceedings of the IEEE 1966, 54, 842.
[28] C.H. Seager, D.C. McIntyre, W.L. Warren, B.A. Tuttle, Applied Physics Letters 1996, 68, 2660.
[29] T.P. Ma, J.-P. Han, IEEE Electron Device Letters 2002, 23, 386.
[30] P. Wurfel, I.P. Batra, Physical Review B 1973, 8, 5126.